

Article

# Nowotny Chimney Ladder Phases with Group 5 Metals: Crystal and Electronic Structure and Relations to the CrSi<sub>2</sub> Structure Type

Maxim S. Likhanov <sup>1,\*</sup>, Nikita V. Sytov <sup>1</sup>, Zheng Wei <sup>2</sup>, Evgeny V. Dikarev <sup>2</sup> and Andrei V. Shevelkov <sup>1</sup>

<sup>1</sup> Department of Chemistry, Lomonosov Moscow State University, 119991 Moscow, Russia; sytovn@yandex.ru (N.V.S.); shev@inorg.chem.msu.ru (A.V.S.)

<sup>2</sup> Department of Chemistry, University at Albany, SUNY, Albany, NY 12222, USA; zwei@albany.edu (Z.W.); edikarev@albany.edu (E.V.D.)

\* Correspondence: likhanov@inorg.chem.msu.ru

Received: 18 July 2020; Accepted: 2 August 2020; Published: 3 August 2020



**Abstract:** Nowotny chimney ladder (NCL) phases are intermetallic compounds formed by transition metals and metals of groups 13 and 14. This family can be expanded by combining two *p*-elements from different groups with those transition metals, for which the corresponding binary NCL phases are unknown. In this paper, we present three new compounds in the V-Al-Ge, Nb-Al-Ge, and Nb-Ga-Ge systems related to the TiSi<sub>2</sub> structure type (Sp. Gr. *Fddd*) obtained with the standard ampule technique. The crystal structures of the new compounds were determined using synchrotron powder X-ray diffraction data. A transition to the CrSi<sub>2</sub> structure type was detected upon changing the composition from VAl<sub>0.72(2)</sub>Ge<sub>1.28(2)</sub> to VAl<sub>1.534(3)</sub>Ge<sub>0.466(3)</sub>. According to the 18-*n* rule, all the compounds are metallic conductors, which was supported by the electronic structure calculations. It was shown that the expected energy gap located above the Fermi level in the vanadium-based NCL compound collapsed into a pseudogap upon the replacement of V by Nb.

**Keywords:** Nowotny chimney-ladder phases; intermetallic compounds; crystal structure; electronic structure

## 1. Introduction

Intermetallics are a large class of compounds with a variety of crystal structures. Most of the metals in the Periodic Table allow for diverse combinations, which lead to a wealth of crystal and electronic structures [1–3]. Their diversity ensures a plethora of properties; as a result, intermetallic compounds are widely used in technology and are also an object of basic scientific interest [4–6]. For intermetallics, there is still no general theory that links their composition, structure, and properties [6]. This is not surprising; indeed, depending on the nature of the constituent chemical elements and details of the electronic structures, intermetallic compounds can be classified into three major groups. The extreme cases are represented by, on one side, ionic compounds such as Zintl phases with an almost complete charge transfer between cationic and anionic substructures and, on the opposite side, so-called electronic compounds such as Hume–Rothery phases with almost no charge transfer. For both groups, elaborate approaches have been devised to relate their crystal and electronic structures with properties [7,8]. Polar intermetallics are an intermediate case, which itself represents a heterogeneous field of multifarious structural and bonding patterns. It includes intermetallic compounds formed by metals from different blocks of the Periodic Table: transition metals on one side and metals or semimetals of the *p*-block on the other side. The so-called Nowotny chimney ladder (NCL) phases belong to this subclass of polar intermetallic compounds.

NCL phases are widely known and crystallize in more than 10 structure types [9–16]. Despite the variety of the crystal structures, they all have common dominant features. Transition metal atoms form a four-step helix that opens up in the form of a channel with a square base (slightly distorted in the case of  $\text{TiSi}_2$ ), inside which atoms of a  $p$ -metal/semimetal form spirals of different repeat intervals, depending on the stoichiometry of a phase. Channels of transition metal atoms resemble a “chimney”, inside of which there are spiral-shaped “ladders” made of  $p$ -element atoms (see Figure 1a,b).

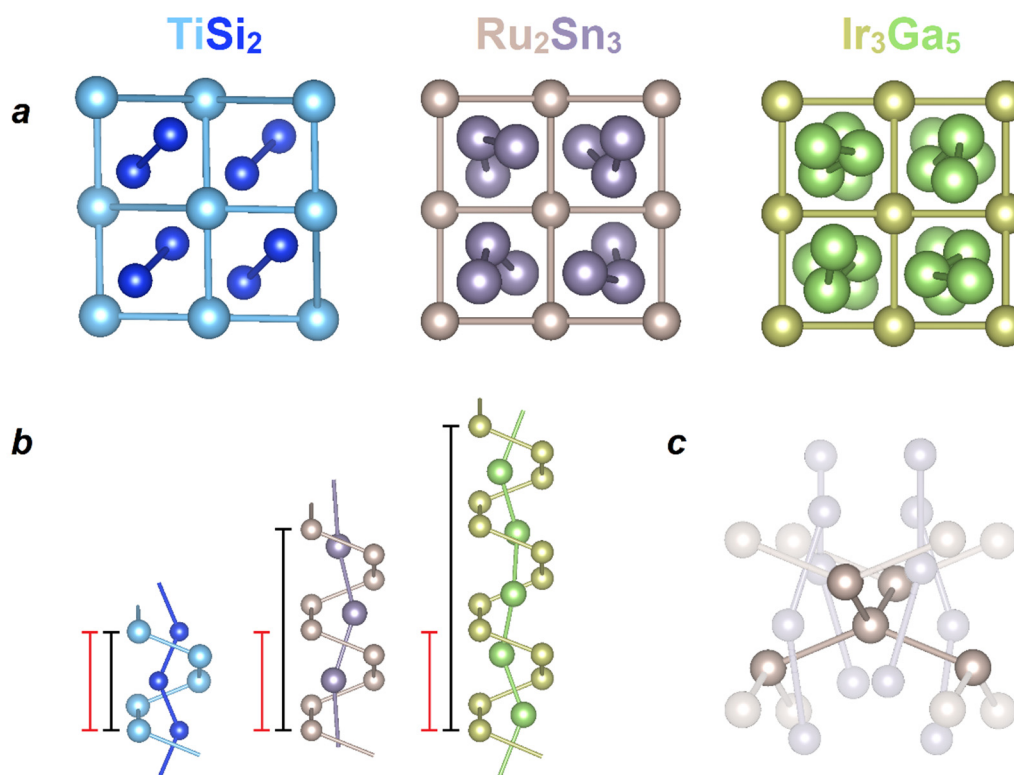


**Figure 1.** Crystal structures of Nowotny chimney ladder (NCL) phases exemplified by  $\text{TiSi}_2$ ,  $\text{Ru}_2\text{Sn}_3$ , and  $\text{Ir}_3\text{Ga}_5$  structure types. (a) View of the structures perpendicular to the  $d$ - and  $p$ -helices. (b)  $p$ -element helical “ladder” inside a transition metal “chimney” with periodicity (repeating periods of  $d$ -metal and  $p$ -element are shown by red and black lines, respectively). (c) Four shortest metal–metal interactions between the transition metal atoms in the NCL phases of the  $\text{Ru}_2\text{Sn}_3$  crystal structure.

Another common feature of the NCL phases is the deviation from the stoichiometric composition, which leads to the formation of incommensurate structures due to the mismatch of the repeating periods of  $d$ - and  $p$ -helices. For many such compounds, the corresponding approximant structures have been proposed. Thus, single crystals of  $\text{Fe}_2\text{Ge}_3$  possess a precise composition and commensurate structure, while a polycrystalline sample is characterized by a complex incommensurate crystal structure [10–12]. In addition, helices can be formed by more than one element. It should be noted that employing a combination of two  $p$ -elements allows one to obtain new NCL phases for some of the transition metals that do not form binary NCL phases. According to this approach, phases with the  $\text{TiSi}_2$  structure type have been obtained in the Cr–Al–Ge, Mo–Ga–Ge, Mn–Al–Si, Nb–Al–Si, Mo–Al–Ge, and Mo–Al–Si systems, despite the absence of binary compounds for those  $d$ -metals involved [17–22]. One more important feature of the NCL phases is the valence electron count (VEC), which varies within the range of 12 to 14 per transition element atom, with possible minor deviations to slightly higher values, such as for  $\text{Rh}_{17}\text{Ge}_{22}$  (VEC = 14.18) [23]. Noteworthy is a unique case of  $hp$ - $\text{Co}_2\text{Si}_3$  (VEC = 15); however, this compound can be prepared only at a high pressure of 7 GPa [24]. Based on the crystal and electronic structures of NCL phases, the 14-electron rule has been formulated [9,15,16], which was later transformed into the  $18-n$  rule [25,26]. According to it, in polar intermetallic compounds based

on transition metals, the VEC should adhere to  $18-n$ , where  $n$  is the number of electron pairs shared between transition metal atoms, which corresponds to the number of  $d$ -M- $d$ -M bonds. This number is 4 for all NCL phases according to the features of their crystal structure (see Figure 1c). In addition, the formation of a gap or a pseudogap at the Fermi level is frequently observed at VEC = 14. However, a sizable number of phases are electron-poor but nonetheless stable [26].

To date, only two NCL phases with group 5 metals are known; they are binary  $V_{17}Ge_{31}$  [27] and ternary  $NbAl_{0.6}Si_{1.4}$  [19]; the latter compound is found to crystallize in the  $TiSi_2$  structure type.

The major goal of this work was the targeted synthesis of NCL phases with the  $TiSi_2$ -type in systems where vanadium or niobium is employed as a transition metal forming a “chimney”, and a combination of two elements of groups 13 and 14 is used as a  $p$ -element-building “ladder”: in this case, aluminum and germanium or gallium and germanium. The compositional range of the phases’ existence and their crystal structures were investigated experimentally, and the electronic structure of the new compounds was calculated.

## 2. Materials and Methods

### 2.1. Synthesis

Chips of metallic vanadium (99.9%), powder of niobium (99.98%), germanium chips (99.9999%), and gallium ingots (99.9999%) were used as starting materials. Before application, vanadium was treated with a diluted (2%) solution of hydrochloric acid to remove an oxide film from the metal surface. A stoichiometric mixture of the elements was loaded into a quartz ampule, which was evacuated (residual pressure of  $1 \times 10^{-3}$  Torr) and sealed. Ampules were annealed at 750 °C for one week, after which the samples were ground, pressed into pellets, and annealed under the same conditions for another week. For the synthesis, the following stoichiometric ratios were used:  $VAl_{2-x}Ge_x$  ( $x = 0.8, 0.9, 1, 1.1, 1.2, 1.3, 1.4, 1.5$ ),  $VGa_{2-x}Ge_x$  ( $x = 0.5, 0.7, 0.8, 0.9, 1, 1.1, 1.2, 1.3, 1.5$ ),  $NbAl_{2-x}Ge_x$  ( $x = 0.5, 0.7, 0.8, 0.9, 1, 1.1, 1.2, 1.3, 1.5$ ), and  $NbGa_{2-x}Ge_x$  ( $x = 0.8, 0.9, 1, 1.1, 1.2, 1.3, 1.4$ ).

Single crystals of  $VAl_{2-x}Ge_x$  were grown using chemical transport reactions with several crystals of  $I_2$  as a transport agent. A pre-synthesized phase-pure polycrystalline sample of  $VAl_{2-x}Ge_x$  was annealed in an evacuated quartz ampule in a two-zone horizontal furnace for 14 days. The load temperature was 450 °C, while the crystallization zone was kept at 400 °C.

### 2.2. Powder X-ray Diffraction

The phase composition of all the products was determined by powder X-ray diffraction (PXRD) analysis using a Huber G670 Guinier Camera (Cu  $K\alpha_1$  radiation, Ge monochromator,  $\lambda = 1.5406$  Å). The data were collected by scanning the image plate 4 times after an exposure time of 2400 s at room temperature.

### 2.3. Energy Dispersive X-ray Analysis

A scanning electron microscope, JSM JEOL 6490-LV, equipped with an energy dispersive X-ray (EDX) analysis system, INCA x-Sight, was used for the chemical analysis. The accelerating voltage was 30 kV. The uncertainty of the measurements for each element was 1 at.%. For the measurements, the samples were finely ground and pressed into pellets. The detailed EDX analysis results as well as EDX mapping are shown in the Table S1 and Figure S1 of the Supplementary Materials.

### 2.4. Crystal Structure Investigation

The crystal structures of the phase-pure samples with the nominal composition  $VAl_{0.7}Ge_{1.3}$  and  $NbGa_{0.8}Ge_{1.2}$  were investigated using high-resolution PXRD data collected at the ID22 beamline of the European Synchrotron Radiation Facility (ESRF, Grenoble, France) ( $\lambda = 0.35451$  Å,  $2\theta$  range of  $1-37.914^\circ$ , and a scan step of  $0.002^\circ$ ). Room temperature measurements were performed on the samples enclosed in sealed quartz capillaries with an inner diameter of 0.5 or 0.2 mm. The capillaries were

spun during the measurements. The Jana 2006 software was used for the structure refinement [28]. The PXRD patterns are presented in Figure S2 of the Supplementary Materials.

Single crystals of  $\text{VAl}_{2-x}\text{Ge}_x$  grown from a single-phase  $\text{VAl}_{0.7}\text{Ge}_{1.3}$  polycrystalline sample were investigated at 100 K on a Bruker D8 VENTURE single-crystal X-ray diffractometer equipped with a PHOTON 100 CMOS detector, graphite monochromator, and Mo-target X-ray tube ( $\lambda = 0.73071 \text{ \AA}$ ). A frame width of  $0.50^\circ$  and exposure time of 15 s/frame were employed for data collection. Data reduction and integration were performed with the Bruker software package SAINT (Version 8.38A) [29]. The absorption correction was performed using the multiscan routine as implemented in SADABS (Version 2014/5) [30,31]. The crystal structure was solved by the charge-flipping algorithm using the Superflip program [32]. Furthermore, the data were refined in the full-matrix anisotropic approximation against  $|F^2|$  using the SHELXTL (Version 2017/1) program package [33]. The crystal structures were visualized using the VESTA 3 package [34].

Crystallographic data as well as structure solution and refinement details are presented in Tables 1 and 2. CCDC/CSD 2017189, 2017190, and 2017191 contain the supplementary crystallographic data for this paper. These data can be obtained free of charge at [www.ccdc.cam.ac.uk/data\\_request/cif](http://www.ccdc.cam.ac.uk/data_request/cif), by emailing [data\\_request@ccdc.cam.ac.uk](mailto:data_request@ccdc.cam.ac.uk), or by contacting The Cambridge Crystallographic Data Centre, 12 Union Road, Cambridge CB2 1EZ, UK; fax: +44 1223 336033.

**Table 1.** Crystallographic data and structure refinement parameters for  $\text{VAl}_{2-x}\text{Ge}_x$  and  $\text{NbGa}_{2-x}\text{Ge}_x$  powder samples.

Sample	$\text{VAl}_{2-x}\text{Ge}_x$	$\text{NbGa}_{2-x}\text{Ge}_x$
Nominal composition	$\text{VAl}_{0.7}\text{Ge}_{1.3}$	$\text{NbGa}_{0.8}\text{Ge}_{1.2}$
Refinement composition	$\text{VAl}_{0.72(2)}\text{Ge}_{1.28(2)}$	$\text{NbGa}_{0.8}\text{Ge}_{1.2}^*$
Molar mass, g/mol	163.4	235.80
Structure type	$\text{TiSi}_2$	$\text{TiSi}_2$
Space group	<i>Fddd</i>	<i>Fddd</i>
Z	8	8
<i>a</i> , Å	4.87415(5)	5.05858(3)
<i>b</i> , Å	8.33502(9)	8.61295(6)
<i>c</i> , Å	8.70267(9)	8.92618(6)
<i>V</i> , Å <sup>3</sup>	353.556(7)	388.907(4)
<i>d</i> <sub>calc</sub> , g/cm <sup>3</sup>	6.140	8.054
Temperature, K	293	293
Radiation, λ, Å	Synchrotron, 0.35451	Synchrotron, 0.35451
2θ range, °	1–37.914	1–37.914
Total No. of reflections	287	318
No. of refined parameters	32	27
<i>R</i> <sub>1</sub>	0.0441	0.0807
<i>wR</i> <sub>2</sub>	0.0602	0.0817
<i>R</i> <sub>prof</sub>	0.0637	0.0871
<i>wR</i> <sub>prof</sub>	0.1435	0.1728
GoF	2.94	2.89

\* The ratio of gallium and germanium was fixed according to the nominal composition.

**Table 2.** Crystallographic data and refinement parameters for  $\text{VAl}_{2-x}\text{Ge}_x$  single-crystal X-ray diffraction.

Sample	$\text{VAl}_{2-x}\text{Ge}_x$
Refinement composition	$\text{VAl}_{1.534(3)}\text{Ge}_{0.466(3)}$
Molar mass, g/mol	126.18
Structure type	$\text{CrSi}_2$
Space group	<i>P</i> <sub>6</sub> <sub>4</sub> <sub>22</sub>
Z	3
<i>a</i> , Å	4.6178(2)
<i>c</i> , Å	6.4218(4)

Table 2. Cont.

Sample	VAl <sub>2-x</sub> Ge <sub>x</sub>
$V, \text{\AA}^3$	118.593(13)
$d_{\text{calc}}, \text{g/cm}^3$	5.300
Temperature, K	100
$\mu, \text{mm}^{-1}$	15.168
Radiation, $\lambda, \text{\AA}$	Mo K $\alpha$ , 0.71073
Absorption correction	Multiscan
$\theta$ range, $^\circ$	3.172–38.571
Index ranges	$-8 \leq h \leq 8; -8 \leq k \leq 8; -11 \leq l \leq 11$
No. of reflections collected	4776
No. unique/no. observed [ $I > 2\sigma(I)$ ]	227/224
$T_{\text{min}}/T_{\text{max}}$	0.186/0.320
No. of refined parameters	12
$R_1 [I > 2\sigma(I)]$	0.0156
$wR_2 [I > 2\sigma(I)]$	0.0463
GoF	1.616

### 2.5. Electronic Structure Calculations

The atomic coordinates and unit cell parameters obtained from the crystal structure refinement were used for electronic structure calculations within the density functional theory (DFT) approach using a Full-Potential Local-Orbital minimum basis band-structure (FPLO) code (version 14.00-47) [35]. The local density approximation (LDA) functional was used to treat the exchange-correlation energy in the fully relativistic regime [36]. Integrations in the  $k$ -space were performed with an improved tetrahedron method [37] on a grid of  $16 \times 16 \times 16$   $k$ -points.

Since, according to the crystal structure solution data, the formation of a superstructure or ordering of aluminum/gallium and germanium in a single  $p$ -element position was not found for all phases, we proposed several ordered models for the electronic structure calculations. A schematic representation of all the models is shown in Figure 2a,b: three models for the TiSi<sub>2</sub>-structure type and two models for the CrSi<sub>2</sub>-structure type. Despite the fact that the refined compositions of the new phases are different from the M:E1:E2 = 1:1:1 (M = V, Nb; E1 = Al, Ga; E2 = Ge) ratio, we used this integer stoichiometry in order to simplify the band structure calculations and to perform a qualitative comparison of the results for the different models against each other.

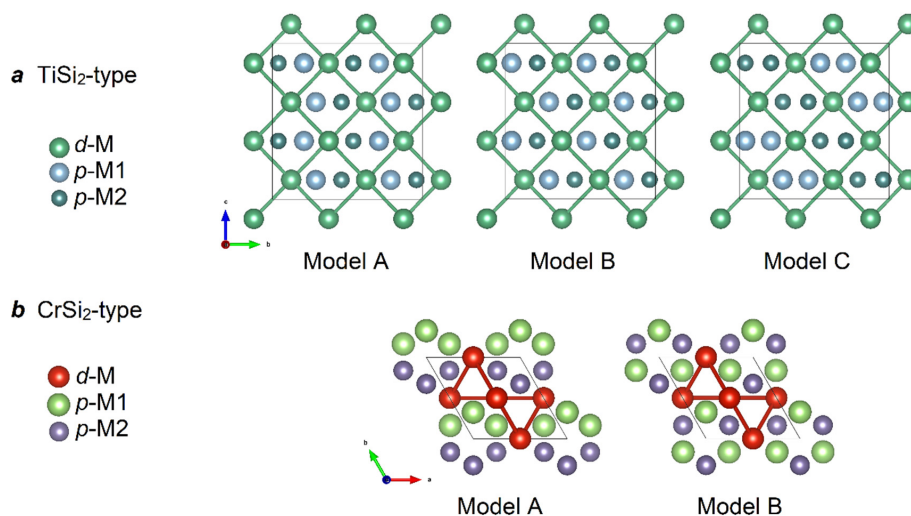


**Figure 2.** Schematic representation of ordered models for band structure calculations. The black frame shows the unit cell. (a) TiSi<sub>2</sub>-type; in the case of VAlGe,  $d\text{-M} = \text{V}$ ,  $p\text{-M1} = \text{Al}$ ,  $p\text{-M2} = \text{Ge}$ ; for NbGaGe,  $d\text{-M} = \text{Nb}$ ,  $p\text{-M1} = \text{Ga}$ ,  $p\text{-M2} = \text{Ge}$ . (b) CrSi<sub>2</sub>-type; for VAlGe,  $d\text{-M} = \text{V}$ ,  $p\text{-M1} = \text{Al}$ ,  $p\text{-M2} = \text{Ge}$ .

In addition, a virtual crystal approximation (VCA) was used for the  $\text{NbGa}_{2-x}\text{Ge}_x$  phase. In this case, we could freely vary the nuclear charge of the  $p$ -element from the ideal composition of the ordered models ( $\text{NbGaGe}$ ,  $p$ -element nuclear charge of 31.5) to the real one ( $\text{NbGa}_{0.8}\text{Ge}_{1.2}$ ,  $p$ -element nuclear charge of 31.6).

### 3. Results and Discussion

#### 3.1. $\text{VAI}_{2-x}\text{Ge}_x$ : Phase Equilibria, and Crystal and Electronic Structure

All  $\text{VAI}_{2-x}\text{Ge}_x$  ( $x = 0.8, 0.9, 1, 1.1, 1.2, 1.3, 1.4, 1.5$ ) samples were investigated by the PXRD analysis, according to which we observed the formation of a new compound in the region of  $x$  between 0.9 and 1.5. A phase-pure sample was obtained for the  $\text{VAI}_{0.7}\text{Ge}_{1.3}$  nominal composition, for which all reflections on the diffraction pattern were indexed in the orthorhombic crystal system (Sp. Gr.  $Fddd$ ), and the composition  $\text{V}_{1.02(3)}\text{Al}_{0.72(3)}\text{Ge}_{1.26(3)}$  was confirmed by the EDX analysis (for details, see Figure S1). An increase in the germanium content ( $x \geq 1.4$ ) in the samples leads to the formation of a second phase— $\text{VGe}_2$  (CrSi<sub>2</sub>-type, Sp. Gr.  $P6_222$  [38])—as an impurity. At the same time, the amount of the target phase decreases. With a decrease in the germanium content ( $1 \leq x \leq 1.2$ ), a decrease in the amount of the target compound and the formation of impurity phases  $\text{V}_5\text{Ge}_3$  ( $\text{W}_5\text{Si}_3$ -type, Sp. Gr.  $I4/mcm$  [39]) and  $\text{VAI}_3$  ( $\text{TiAl}_3$ -type, Sp. Gr.  $I4/mmm$  [40]) are observed. Finally, reflections of the new compound are not detected at the lowest investigated germanium content ( $x \leq 0.9$ ). An illustration of the phase composition change for the  $\text{VAI}_{2-x}\text{Ge}_x$  series is shown in Figure 3.

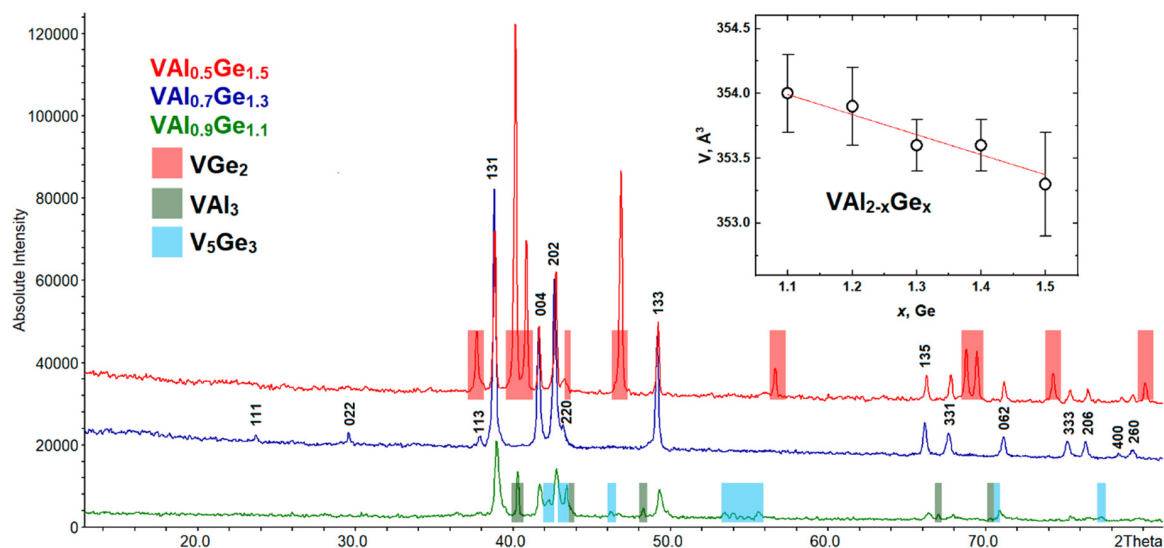


**Figure 3.** Powder X-ray diffraction (PXRD) patterns of  $\text{VAI}_{2-x}\text{Ge}_x$  ( $x = 1.1, 1.3, \text{ and } 1.5$ ). Inset: the unit cell volume of  $\text{VAI}_{2-x}\text{Ge}_x$  ( $Fddd$ ) vs. nominal Ge content.

It should be noted that the calculated unit cell parameters change only slightly with the nominal composition (see the inset of Figure 3), pointing at a narrow homogeneity range of the new compound, whose width could not be detected with reasonable accuracy.

A single-phase powder sample  $\text{VAI}_{0.7}\text{Ge}_{1.3}$  was investigated using synchrotron PXRD, and the crystal structure was refined (Table 1). As expected, the new compound crystallizes in the  $\text{TiSi}_2$  structure type (Sp. Gr.  $Fddd$ ) and belongs to the family of NCL phases. There are two unique positions in the crystal structure—one for vanadium and another for  $p$ -elements. No ordering of aluminum and germanium was observed; thus, there is a statistical population of the  $p$ -M1 site by Al and Ge with a refined occupancy equal to  $0.36(2)\text{Al} + 0.64(2)\text{Ge}$ , which yields the  $\text{VAI}_{0.72(2)}\text{Ge}_{1.28(2)}$  composition, in perfect agreement with the EDX data. The mixed population of the  $16f$  site by two  $p$ -elements is typical for the NCL phases with the  $\text{TiSi}_2$  crystal structure, even when  $p$ -elements with different atomic

radii are combined [17,20]. The atomic parameters for the crystal structure of  $\text{VAl}_{0.72(2)}\text{Ge}_{1.28(2)}$  are presented in Table 3.

**Table 3.** Atomic coordinates and thermal displacement parameters of the  $\text{VAl}_{0.72(2)}\text{Ge}_{1.28(2)}$ .

Atom	Wyckoff Site	$x/a$	$y/b$	$z/c$	$U_{\text{iso}}, \text{\AA}^2$	Occupancy
V1	8a	0.125	0.125	0.125	0.0093(12)	1
<i>p</i> -M1	16 <i>f</i>	0.125	0.4562(3)	0.125	0.0068(5)	0.36(2)Al + 0.64(2)Ge

The obtained phase-pure powder of  $\text{VAl}_{0.7}\text{Ge}_{1.3}$  was used for growing crystals exploiting chemical transport reactions in a temperature gradient of 450–400 °C, with iodine serving as a transport agent. Surprisingly,  $\text{VAl}_{1.534(3)}\text{Ge}_{0.466(3)}$  crystals with a  $\text{CrSi}_2$  structure were obtained, and, as can be seen, the refined composition of the single crystal differs greatly from the composition of the initial sample (for details, see Table 2). This is actually an unexpected result. In the V–Al and V–Ge binary systems, there is only one  $\text{CrSi}_2$ -type phase— $\text{VGe}_2$ , which was obtained under high pressure conditions [38]. Apparently, in our case, phase stabilization occurs due to the substitution of part of the germanium atoms by aluminum atoms, and then we could expect that the “ $\text{VGe}_2$ ” phase that we detected analyzing XRD patterns (see Figure 3) may also contain aluminum, although no especial studies have been carried out in this work. Although the refined composition of the grown crystals is very rich in aluminum ( $\text{VAl}_{1.534(3)}\text{Ge}_{0.466(3)}$ ), this compound crystallizes in the  $\text{CrSi}_2$  structure type, whereas isostructural  $\text{VAl}_{0.66}\text{Si}_{1.34}$ , on the contrary, has a reduced content of a group 13 metal [41]. Thus, the transition from the  $\text{TiSi}_2$  structure type to the  $\text{CrSi}_2$ -type strongly depends on both the nominal composition and synthetic conditions. At 750 °C,  $\text{VAl}_{0.72(2)}\text{Ge}_{1.28(2)}$  that crystallizes in the  $\text{TiSi}_2$  structure type is synthesized, while the increasing of the germanium content leads to “ $\text{VGe}_2$ ” with the  $\text{CrSi}_2$  structure, which probably contains Al. Crystal growth from  $\text{VAl}_{0.72(2)}\text{Ge}_{1.72(2)}$  powder with iodine as a transport agent at 400 °C leads to the formation of  $\text{VAl}_{1.534(3)}\text{Ge}_{0.466(3)}$  that crystallizes in the  $\text{CrSi}_2$  structure type. Note that the temperature of 400 °C is too low to achieve interaction in the V–Al–Ge system.

The atomic parameters for the  $\text{VAl}_{1.534(3)}\text{Ge}_{0.466(3)}$  crystal structure are presented in Table 4.

**Table 4.** Atomic coordinates and displacement parameters for  $\text{VAl}_{1.534(3)}\text{Ge}_{0.466(3)}$ .

Atom	Wyckoff Site	$x/a$	$y/b$	$z/c$	$U_{\text{eq}}, \text{\AA}^2$	Occupancy
V1	3 <i>c</i>	0.5	0	0	0.00121(12)	1.000
<i>p</i> -M1	6 <i>i</i>	0.16358(2)	0.32716(5)	0	0.00066(15)	0.767(2)Al + 0.233(2)Ge

As a matter of fact, both structure types are very close to each other. A comparison of the two structures is shown in Figure 4a–c. Clearly, the  $\text{CrSi}_2$  structure also contains a “chimney” formed by vanadium atoms, inside which the ladder of silicon atoms is located (Figure 4b). The difference lies in the shift of these “chimneys” relative to each other along the *a* axis by half of the *a* parameter. Other structural differences are minimal. In both  $\text{VAl}_{2-x}\text{Ge}_x$  modifications— $\text{VAl}_{0.72(2)}\text{Ge}_{1.28(2)}$  ( $\text{TiSi}_2$ -type) and  $\text{VAl}_{1.534(3)}\text{Ge}_{0.466(3)}$  ( $\text{CrSi}_2$ -type)—the environment of the vanadium atoms is equivalent and is shown in Figure 4c. Analysis of the crystal structures indicates the presence of four V–V interactions per vanadium atom in both structures, while the systems of *p*-element bonds orthogonal to the transition metal are absent. According to the 18–*n* rule, both structure types should have a valence electron count of 14 to be stable and demonstrate properties of a semiconductor [26]. New compounds possess VEC values smaller than 14: 12.28 for  $\text{VAl}_{0.72(2)}\text{Ge}_{1.28(2)}$  ( $\text{TiSi}_2$ -type) and 11.47 for  $\text{VAl}_{1.534(3)}\text{Ge}_{0.466(3)}$  ( $\text{CrSi}_2$ -type). Nevertheless, for both structure types, a reduced VEC value is not uncommon, and the compounds exhibit a metallic character of conductivity. Moreover, to the best of our knowledge,  $\text{VAl}_{1.534(3)}\text{Ge}_{0.466(3)}$  is the first representative of the  $\text{CrSi}_2$  structure type that has a VEC lower than 12.

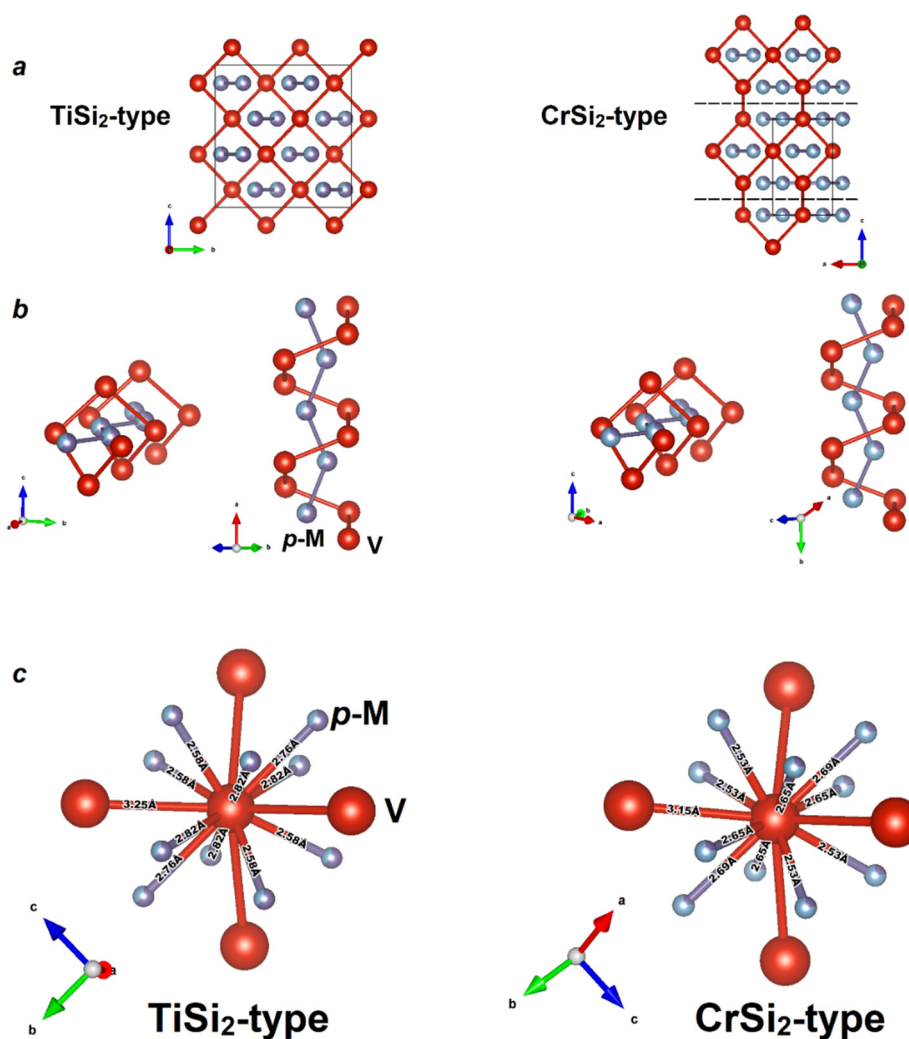


**Figure 4.** Comparison of the crystal structures of the  $\text{VAI}_{2-x}\text{Ge}_x$ —TiSi<sub>2</sub>-type for  $x = 1.28(2)$  and CrSi<sub>2</sub>-type for  $x = 0.466(3)$ : (a) a general view of the crystal structures; (b) equivalence of the *d*- and *p*-metal helices in both structures; (c) local environment of vanadium atoms.

According to the values of VEC, the new compounds  $\text{VAI}_{0.72(2)}\text{Ge}_{1.28(2)}$  and  $\text{VAI}_{1.534(3)}\text{Ge}_{0.466(3)}$  should be metallic conductors. To confirm this assumption, we performed electronic structure calculations. It should be noted that the ideal composition  $\text{VAIGe}$  was used for the calculations because it was not possible to apply the virtual crystal approximation (VCA) for accounting for the non-integer occupancy factors of two *p*-elements from different periods.

The calculated electronic structure near the Fermi level for  $\text{VAIGe}$  (TiSi<sub>2</sub>-type) is presented in Figure 5 for all ordered models. All the selected ordered models show qualitatively identical results. Clearly,  $\text{VAIGe}$  should have a metallic type of electrical conductivity, since a nonzero density of states (DOS) is found at the Fermi level. As expected, the band gap is located above the Fermi level, the value of which varies from 0.37 to 0.43 eV, depending on the ordering model. The main contribution to the DOS around the gap is made by the states of vanadium and, to a lesser extent, the states of aluminum and germanium. The same can be said about the states near the Fermi level: vanadium makes the main contribution to the DOS, and approximately equal contributions are observed from aluminum and germanium; the latter are approximately 2–3 times smaller than those from vanadium.

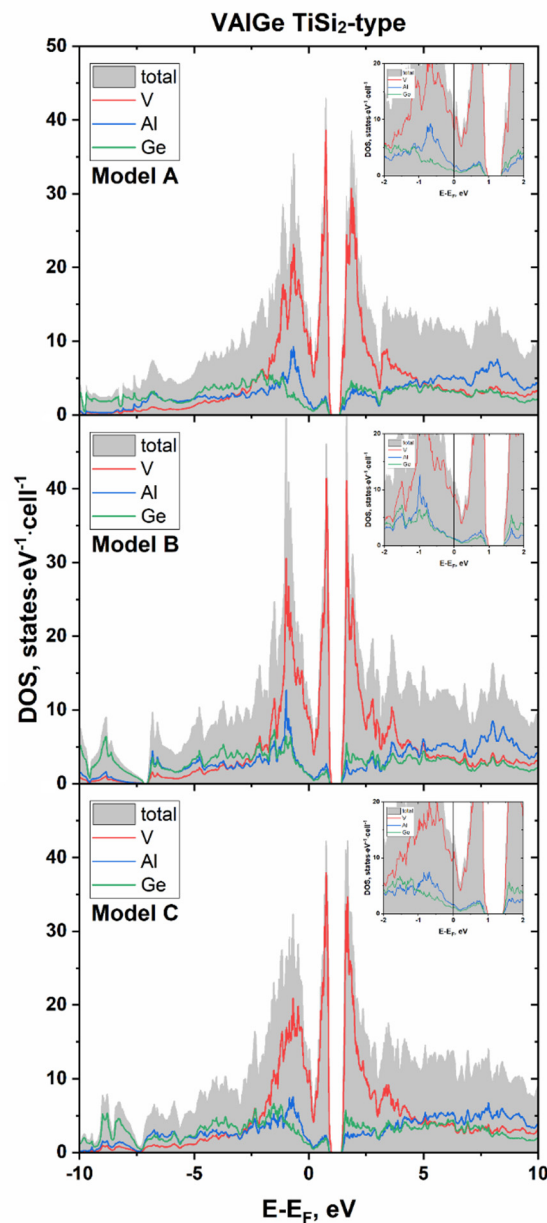


**Figure 5.** Calculated total and projected density of states (DOS) near Fermi level for ordered models of VAiGe with the TiSi<sub>2</sub> structure type.

The integration of the DOS region from the Fermi level to the band gap gives exactly two electrons per formula unit, yielding an expected  $14\text{-}\bar{e}$  phase, which is consistent with the  $18\text{-}n$  rule. Since the VAiGe ideal composition has a VEC value of 12, according to the  $18\text{-}n$  rule, the VEC should be equal to 14 in order to realize a semiconducting state.

An interesting feature is the presence of a pronounced deep minimum located just above the Fermi level and well below the gap (see the insets in Figure 5). The integration of the DOS region between the dip and the Fermi level yields 0.24–0.26 electrons per formula for different models, which nicely matches the actual composition VA<sub>1.72(2)</sub>Ge<sub>1.28(2)</sub> (12 + 0.28 electrons). We can assume that the deviation of the VA<sub>2-x</sub>Ge<sub>x</sub> actual composition from the ideal  $12\text{-}\bar{e}$  configuration and the very narrow homogeneity range stem from the tendency to reach the local energy minimum that corresponds to the dip in the DOS.

Apparently, the presence of such a minimum (pseudogap) below the band gap ensures the existence of many electron-poor phases that demonstrate a VEC lower than that predicted by the

18– $n$  rule [26]. The states slightly below the energy gap are usually non-bonding orbitals of the transition metal in such compounds; therefore, a large number of electron-poor phases becomes unsurprising. We especially observe this fact for related structure types of disilicides: TiSi<sub>2</sub>-type (TiSi<sub>2</sub>, TiGe<sub>2</sub>, and ZrSn<sub>2</sub> VEC = 12; CrAlGe VEC = 13), CrSi<sub>2</sub>-type (VSi<sub>2</sub>, VGe<sub>2</sub>, NbSi<sub>2</sub>, NbGe<sub>2</sub>, TaSi<sub>2</sub>, TaGe<sub>2</sub>, CrAlSi, MoAlGe, and MoAlSi VEC = 13), and ZrSi<sub>2</sub>-type (ScGe<sub>2</sub> and YGe<sub>2</sub> VEC = 11; TiSi<sub>2</sub>, ZrSi<sub>2</sub>, ZrGe<sub>2</sub>, and HfSi<sub>2</sub> VEC = 12) [14,17,20,21,41–51].

Similar results were obtained from the electronic structure calculations for VAlGe with the CrSi<sub>2</sub>-type (see Figure 6). The Fermi level is located in the valence band, where the main contribution comes from the states of vanadium. Exactly two electrons per formula fit between the Fermi level and the energy gap of the 12- $\bar{e}$  VAlGe, which also agrees with the 18– $n$  rule applied to this structure type [26]. Thus, the 14- $\bar{e}$  compounds CrSi<sub>2</sub>, MoSi<sub>2</sub>, and WSi<sub>2</sub> with the CrSi<sub>2</sub>-type exhibit semiconducting behavior according to theoretical calculations as well as an experimental investigation in the case of CrSi<sub>2</sub> [45,52].

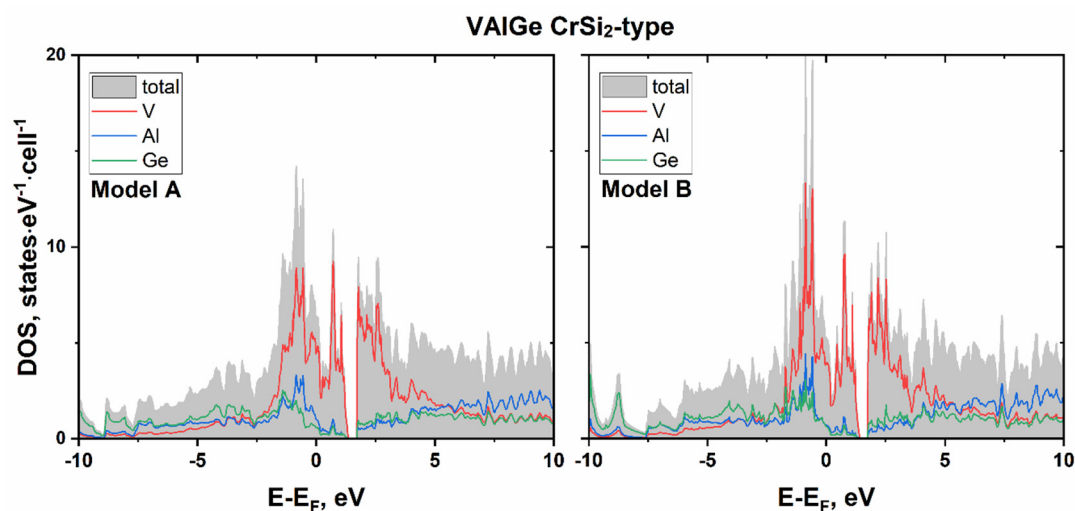


**Figure 6.** Calculated total and projected DOS near Fermi level for VAlGe ordered models in CrSi<sub>2</sub>-type.

We also examined the VGe<sub>2-x</sub>Ge<sub>x</sub> cut in detail and did not detect the existence of an expected phase with the NCL phase crystal structure (the investigated range of  $x$  is given in Section 2.1). Since the aim of this study was precisely the target synthesis of the NCL phase, we do not give a detailed description of the phase relations in this system. In all cases, mixtures of known vanadium germanides and vanadium aluminides were obtained according to PXRD data.

### 3.2. NbE<sub>2-x</sub>Ge<sub>x</sub> (E = Al, Ga): Phase Equilibria, Crystal and Electronic Structure

The same approach was applied to the search for new compounds with the NCL phase structure (TiSi<sub>2</sub>-type) in the systems where niobium was used as a transition metal instead of vanadium, and the combinations of Al/Ge and Ga/Ge were used as a  $p$ -metal/semimetal.

The formation of a new compound, reflections of which are indexed in an orthorhombic unit cell (Sp. Gr. *Fddd*), was detected in the Nb-Al-Ge system for a wide range of  $x$ . Although niobium digermanide NbGe<sub>2</sub> [43] is a main phase at  $x \geq 1.1$ , there are also some amounts of a target phase along with a second side-phase NbAl<sub>3</sub> [26,53]. The new compound and NbAl<sub>3</sub> become the main phases at  $x \leq 1$ , while the maximum intensity of reflections of the target phase is observed at  $x = 1$ . The phase composition change across the NbAl<sub>2-x</sub>Ge<sub>x</sub> series is shown in Figure 7. As can be seen, the NbAl<sub>2-x</sub>Ge<sub>x</sub> cut does not show a region of single-phase NCL phase existence, which might indicate a deficiency of the  $p$ -elements in the desired compound. According to the EDX data, the measured composition of the NCL phase was Nb<sub>1.11(3)</sub>Al<sub>0.57(6)</sub>Ge<sub>1.32(3)</sub> for the sample with the NbAlGe nominal composition (for details, see Table S1 and Figure S1), which might indicate an exit from the NbAl<sub>2-x</sub>Ge<sub>x</sub> cut. We note that our attempts to optimize the synthetic conditions by changing the initial composition and varying

the temperature did not lead to a better yield of the target phase, and the best yield was obtained for the nominal composition NbAlGe. The inset in Figure 7 shows the dependence of the unit cell volume obtained by indexing peaks attributed to the NCL phase. It should be borne in mind that the given composition “NbAl<sub>2-x</sub>Ge<sub>x</sub>” differs from the real one. Nevertheless, the fundamental possibility of obtaining a compound with a crystal structure of the NCL phase (TiSi<sub>2</sub>-type) in the Nb-Al-Ge system was shown.

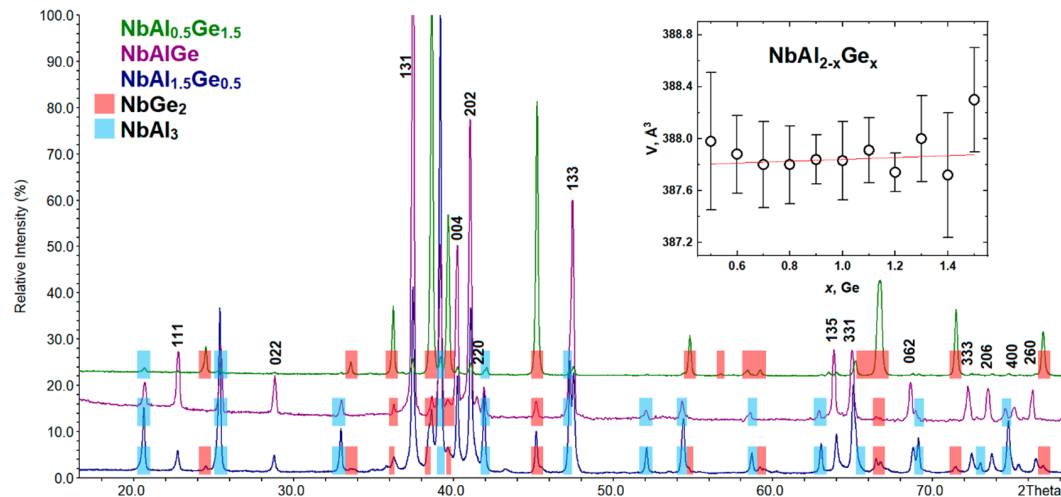


**Figure 7.** PXRD patterns of NbAl<sub>2-x</sub>Ge<sub>x</sub> ( $x = 0.5, 1,$  and  $1.5$ ). Inset: the unit cell volume of the “NbAl<sub>2-x</sub>Ge<sub>x</sub>” (*Fddd*) vs. nominal Ge content.

For the NbGa<sub>2-x</sub>Ge<sub>x</sub> cut, a single-phase sample was synthesized with a NbGa<sub>0.8</sub>Ge<sub>1.2</sub> composition and an orthorhombic unit cell (Sp. Gr. *Fddd*). The measured composition according to the EDX analysis (Nb<sub>0.99(3)</sub>Ga<sub>0.81(3)</sub>Ge<sub>1.20(3)</sub>) perfectly matches the nominal one. NbGe<sub>2</sub> [43] is formed as a main phase at  $x \geq 1.3$ , where the content of a new compound decreases. An increase in the nominal gallium content in the sample leads to the appearance of NbGa<sub>3</sub> [53,54] as an admixture along with an unidentified compound, the intensity of the peaks of which is quite high. The PXRD patterns of the NbGa<sub>2-x</sub>Ge<sub>x</sub> samples are presented in Figure 8. The unit cell parameters of the new compound slightly decrease with increasing nominal germanium content. We can conclude that the NbGa<sub>2-x</sub>Ge<sub>x</sub> (*Fddd*) homogeneity range is very narrow.

For the phase-pure sample of NbGa<sub>0.8</sub>Ge<sub>1.2</sub>, the crystal structure was refined using synchrotron PXRD data (for details, see Table 1). Crystal structure refinement confirmed the TiSi<sub>2</sub> structure type. The occupancies of the unique *p*-element site containing gallium and germanium atoms were fixed according to the nominal composition NbGa<sub>0.8</sub>Ge<sub>1.2</sub>. The atomic parameters for the crystal structure of NbGa<sub>0.8</sub>Ge<sub>1.2</sub> are presented in Table 5.

The crystal structure parameters of NbGa<sub>0.8</sub>Ge<sub>1.2</sub> were used for electronic structure calculations. The calculations were performed for the same models of *p*-elements' ordering as for VAlGe (see Figure 2); in addition, the proximity of gallium and germanium allowed us to carry out the band structure calculation in the VCA approximation (both for the ideal composition NbGaGe and for the actual composition NbGa<sub>0.8</sub>Ge<sub>1.2</sub>). The calculated DOS curves are shown in Figure 9.

According to the calculation results, NbGaGe is the expected metallic conductor. However, the main feature of the NbGaGe band structure for all the models is the absence of an open energy gap. Unlike in the isostructural VAlGe (see above), the opened gap collapses and turns into a pseudogap in NbGaGe. Similar changes in the band pattern are observed with the increasing atomic mass (replacement of vanadium by niobium and aluminum by gallium in our case). For instance, when passing from Ru<sub>2</sub>Ge<sub>3</sub> to Ru<sub>2</sub>Sn<sub>3</sub> (isostructural NCL phases), the gap also closes with the formation of a pseudogap at the Fermi level [9].

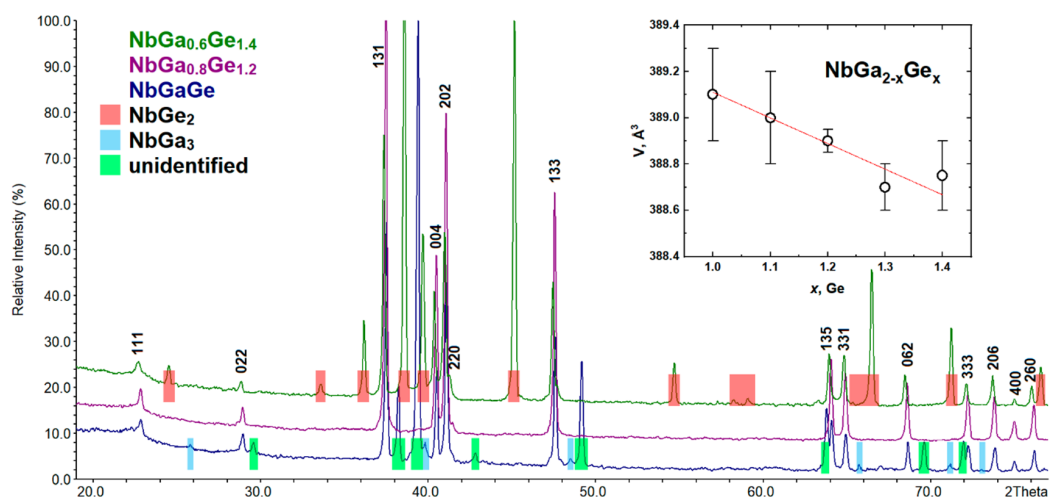


**Figure 8.** PXRD patterns of  $\text{NbGa}_{2-x}\text{Ge}_x$  ( $x = 1, 1.2,$  and  $1.4$ ). Inset: the unit cell volume of the  $\text{NbGa}_{2-x}\text{Ge}_x$  ( $Fddd$ ) vs. nominal Ge content.

**Table 5.** Atomic coordinates and thermal displacement parameters for  $\text{NbGa}_{0.8}\text{Ge}_{1.2}$ .

Atom.	Wyckoff Site	$x/a$	$y/b$	$z/c$	$U_{\text{iso}}, \text{\AA}^2$	Occupancy
Nb1	8a	0.125	0.125	0.125	0.0024(4)	1
$p$ -M1	16f	0.125	0.4604(2)	0.125	0.0066(4)	0.4Ga + 0.6Ge *

\* Fixed according to the nominal composition.

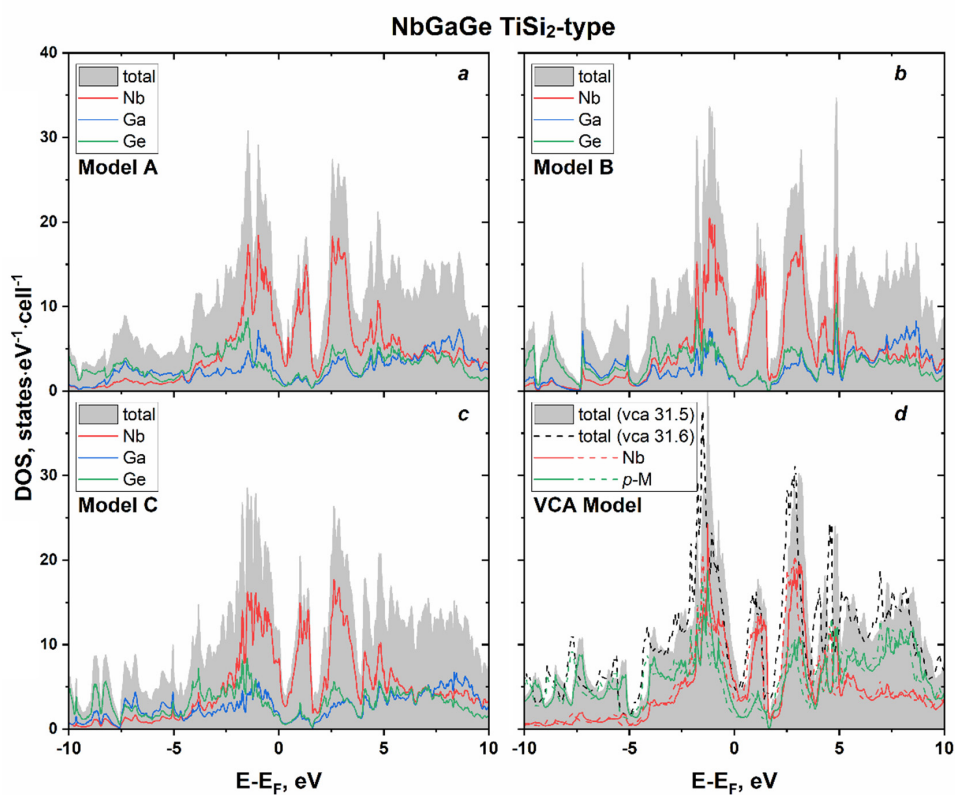


**Figure 9.** Calculated total and projected DOS near Fermi level of  $\text{NbGaGe}$  ( $\text{TiSi}_2$ -type) for ordered models (a–c) and within the virtual crystal approximation (VCA) (d) with  $p$ -M charge 31.5 ( $\text{NbGaGe}$ ) and 31.6 ( $\text{NbGa}_{0.8}\text{Ge}_{1.2}$ ).

The number of electrons found by integrating the DOS region from the Fermi level to the pseudogap is still two (for ordered models and the VCA model with  $p$ -M charge 31.5), which is predicted by the  $18-n$  rule.

#### 4. Conclusions

Three new ternary compounds in the V-Al-Ge, Nb-Al-Ge, and Nb-Ga-Ge systems were synthesized by the standard ampoule technique. All phases belong to the family of Nowotny chimney ladder phases and crystallize in the  $\text{TiSi}_2$  structure type. Two compounds,  $\text{VAl}_{0.7}\text{Ge}_{1.3}$  and  $\text{NbGa}_{0.8}\text{Ge}_{1.2}$ , were obtained as phase-pure powders, and their crystal structures were refined using synchrotron PXRD data. No superstructure was detected, which demonstrates the statistical occupation of a single  $p$ -element site by atoms of groups 13 and 14 without any tendency for ordering. As the respective binary NCL phases are absent, it is plausible to conclude that the formation of new phases is ensured primarily by combining elements of different groups with vanadium or niobium so that the correct VEC is achieved. Crystal growth from the  $\text{VAl}_{0.7}\text{Ge}_{1.3}$  single-phase powder by means of a chemical transport reaction reveals a change in the compound composition ( $\text{VAl}_{1.5}\text{Ge}_{0.5}$ ) with a concomitant transition to the  $\text{CrSi}_2$  structure type that is genetically very close to the NCL  $\text{TiSi}_2$ -type. The calculations of the electronic structures demonstrate metallic properties for all the new compounds, which is in line with the  $18-n$  rule and the corresponding VEC of the new compounds, which is close to 12. In addition, the energy gap in  $\text{VAlGe}$ , which is also predicted by the  $18-n$  rule, degenerates into a pseudogap upon transition to the compound with heavier elements in the case of  $\text{NbGaGe}$ .

**Supplementary Materials:** The following data are available online at <http://www.mdpi.com/2073-4352/10/8/670/s1>. Table S1: EDX analysis results for  $\text{VAl}_{2-x}\text{Ge}_x$ ,  $\text{NbGa}_{2-x}\text{Ge}_x$ , and  $\text{NbAl}_{2-x}\text{Ge}_x$  samples. Figure S1: EDX mapping of the samples with the nominal compositions  $\text{VAl}_{0.7}\text{Ge}_{1.3}$  (a),  $\text{NbGa}_{0.8}\text{Ge}_{1.2}$  (b), and  $\text{NbAlGe}$  (c). (d) comparison of the nominal composition with measured one. Figure S2: Powder X-ray diffraction patterns of  $\text{VAl}_{0.72(2)}\text{Ge}_{1.28(2)}$  (a) and  $\text{NbGa}_{0.8}\text{Ge}_{1.2}$  (b).

**Author Contributions:** Conceptualization, M.S.L. and A.V.S.; formal analysis, M.S.L., N.V.S. and A.V.S.; investigation, M.S.L., N.V.S. and Z.W.; writing—original draft preparation, M.S.L.; writing—review and editing, E.V.D. and A.V.S.; visualization, M.S.L.; supervision, A.V.S.; project administration, A.V.S.; funding acquisition, E.V.D. and A.V.S. All authors have read and agreed to the published version of the manuscript.

**Funding:** The work was supported by the Russian Science Foundation, grant No. 17-13-01033. Z.W. and E.D. thank the National Science Foundation for supporting the structural studies under grant no. CHE-1955585.

**Acknowledgments:** We thank V. Yu. Verchenko for carrying out EDX analysis. We acknowledge ESRF for granting the beam time at ID22 (HC-3841) and thank W. Mogodi for his kind support during the high-resolution XRD measurements.

**Conflicts of Interest:** The authors declare no conflict of interest. The funders had no role in the design of the study; in the collection, analyses, or interpretation of data; in the writing of the manuscript; or in the decision to publish the results.

#### References

1. Steurer, W.; Dshemuchadse, J. *Intermetallics: Structures, Properties, and Statistics*; Oxford University Press: Oxford, UK, 2016.
2. Akhmetshina, T.G.; Blatov, V.A.; Proserpio, D.M.; Shevchenko, A.P. Topology of intermetallic structures: From statistics to rational design. *Acc. Chem. Res.* **2018**, *51*, 21–30. [[CrossRef](#)]
3. Oliynyk, A.O.; Mar, A. Discovery of intermetallic compounds from traditional to machine-learning approaches. *Acc. Chem. Res.* **2018**, *51*, 59–68. [[CrossRef](#)]
4. Buschow, K.H.J. The importance of ternary intermetallic compounds in science and technology. *J. Alloys Compd.* **1993**, *193*, 223–230. [[CrossRef](#)]
5. Fredrickson, D.C.; Miller, G.J. Intermetallic Chemistry: New Advances in Humanity's Age-Old Exploration of Metals and Alloys. *Acc. Chem. Res.* **2018**, *51*, 213. [[CrossRef](#)]
6. Fredrickson, D.C. Parallels in Structural Chemistry between the Molecular and Metallic Realms Revealed by Complex Intermetallic Phases. *Acc. Chem. Res.* **2018**, *51*, 248–257. [[CrossRef](#)] [[PubMed](#)]
7. Mizutani, U. *Hume-Rothery Rules for Structurally Complex Alloy Phases*; CRC Press: New York, NY, USA, 2010.

8. Shevelkov, A.V.; Kovnir, K. *Zintl Clathrates: Structure and Bonding*; Springer: Berlin/Heidelberg, Germany, 2011; Volume 139, pp. 97–142.
9. Imai, Y.; Watanabe, A. Consideration of the validity of the 14 valence electron rule for semiconducting chimney-ladder phase compounds. *Intermetallics* **2005**, *13*, 233–241. [[CrossRef](#)]
10. Verchenko, V.Y.; Wei, Z.; Tsirlin, A.A.; Callaert, C.; Jesche, A.; Hadermann, J.; Dikarev, E.V.; Shevelkov, A.V. Crystal growth of the Nowotny chimney ladder phase  $\text{Fe}_2\text{Ge}_3$ : Exploring new Fe-based narrow-gap semiconductor with promising thermoelectric performance. *Chem. Mater.* **2017**, *29*, 9954–9963. [[CrossRef](#)]
11. Sato, N.; Ouchi, H.; Takagiwa, Y.; Kimura, K. Glass-like Lattice Thermal Conductivity and Thermoelectric Properties of Incommensurate Chimney-Ladder Compound  $\text{FeGe}_\gamma$ . *Chem. Mater.* **2016**, *28*, 529–533. [[CrossRef](#)]
12. Terada, T.; Ishibe, T.; Watanabe, K.; Nakamura, Y. Growth of epitaxial  $\text{FeGe}_\gamma$  nanocrystals with incommensurate Nowotny chimney-ladder phase on Si substrate. *Jpn. J. Appl. Phys.* **2018**, *57*, 08NB01. [[CrossRef](#)]
13. Boström, M.; Lind, H.; Lidin, S.; Niewa, R.; Grin, Y. Synthesis, crystal structure, phase relations and chemical bonding analysis of the new Nowotny chimney-ladder compound  $\text{ZrBi}_{1.62}$ . *Solid State Sci.* **2006**, *8*, 1173–1180. [[CrossRef](#)]
14. Jeitschko, W. Refinement of the crystal structure of  $\text{TiSi}_2$  and some comments on bonding in  $\text{TiSi}_2$  and related compounds. *Acta Crystallogr. B* **1977**, *33*, 2347–2348. [[CrossRef](#)]
15. Fredrickson, D.C.; Lee, S.; Hoffmann, R. The Nowotny chimney ladder phases: Whence the 14 electron rule? *Inorg. Chem.* **2004**, *43*, 6159–6167. [[CrossRef](#)] [[PubMed](#)]
16. Fredrickson, D.C.; Lee, S.; Hoffmann, R.; Lin, J. The Nowotny chimney ladder phases: Following the  $c_{\text{pseudo}}$  clue toward an explanation of the 14 electron rule. *Inorg. Chem.* **2004**, *43*, 6151–6158. [[CrossRef](#)] [[PubMed](#)]
17. Milyan, V.V.; Kuzma, Y.B. Phase equilibria in the Cr-Al-Ge system. *Russ. Metall.* **1987**, *4*, 191–193.
18. Kusma, J.B.; Nowotny, H. Untersuchungen im Dreistoff: Mn-Al-Si. *Monatsh. Chem.* **1964**, *95*, 1266–1271. [[CrossRef](#)]
19. Nowotny, H.; Benesovsky, F.; Brukl, C.E. Der Dreistoff: Niob-Aluminium-Silicium. *Monatsh. Chem.* **1961**, *92*, 193–196. [[CrossRef](#)]
20. Kuzma, Y.B.; Milyan, V.V. New compounds in the system Mo-Al-Ge. *Inorg. Mater.* **1979**, *15*, 11–13.
21. Brukl, C.E.; Nowotny, H.; Schob, O.; Benesovsky, F. Die Kristallstrukturen von  $\text{TiSi}$ ,  $\text{Ti}(\text{Al},\text{Si})_2$  und  $\text{Mo}(\text{Al},\text{Si})_2$ . *Monatsh. Chem.* **1961**, *92*, 781–788. [[CrossRef](#)]
22. Völlenkle, H.; Wittmann, A.; Nowotny, H. Abkömmlinge der  $\text{TiSi}_2$ -Struktur—Ein neues Bauprinzip. *Monatsh. Chem.* **1966**, *97*, 506–516. [[CrossRef](#)]
23. Miyazaki, Y.; Nakajo, T.; Kikuchi, Y.; Hayashi, K. Crystal structure and thermoelectric properties of the incommensurate chimney-ladder compound  $\text{RhGe}_\gamma$  ( $\gamma \sim 1.293$ ). *J. Mater. Res.* **2015**, *30*, 2611–2617. [[CrossRef](#)]
24. Larchev, V.I.; Popova, S.V. The new chimney ladder phases  $\text{Co}_2\text{Si}_3$  and  $\text{Re}_4\text{Ge}_7$  formed by treatment at high temperatures and pressures. *J. Less-Common Met.* **1982**, *84*, 87–91. [[CrossRef](#)]
25. Yannello, V.J.; Fredrickson, D.C. Orbital origins of helices and magic electron counts in the Nowotny chimney ladders: The 18- $n$  rule and a path to incommensurability. *Inorg. Chem.* **2014**, *53*, 10627–10631. [[CrossRef](#)] [[PubMed](#)]
26. Yannello, V.J.; Fredrickson, D.C. Generality of the 18- $n$  rule: Intermetallic structural chemistry explained through isolobal analogies to transition metal complexes. *Inorg. Chem.* **2015**, *54*, 11385–11398. [[CrossRef](#)] [[PubMed](#)]
27. Hamada, H.; Kikuchi, Y.; Hayashi, K.; Miyazaki, Y. Crystal structure and thermoelectric properties of the incommensurate chimney-ladder compound  $\text{VGe}_\gamma$  ( $\gamma \sim 1.82$ ). *J. Electron. Mater.* **2016**, *45*, 1365–1368. [[CrossRef](#)]
28. Petricek, V.; Dusek, M.; Palatinus, L. Crystallographic computing system JANA2006: General features. *Z. Kristallogr. Cryst. Mater.* **2014**, *229*, 345–352. [[CrossRef](#)]
29. Bruker. *SAINTE (Version 8.38A)*; Bruker AXS Inc.: Madison, WI, USA, 2017.
30. Krause, L.; Herbst-Irmer, R.; Sheldrick, G.M.; Stalke, D. Comparison of Silver and Molybdenum Microfocus X-ray Sources for Single-crystal Structure Determination. *J. Appl. Cryst.* **2015**, *48*, 3–10. [[CrossRef](#)]
31. Bruker. *SADABS v. 2014/5*; Bruker AXS Inc.: Madison, WI, USA, 2015.
32. Palatinus, L.; Chapuis, G. Superflip—A computer program for the solution of crystal structures by charge flipping in arbitrary dimensions. *J. Appl. Crystallogr.* **2007**, *40*, 786–790. [[CrossRef](#)]

33. Sheldrick, G.M. Crystal Structure Refinement with SHELXL. *Acta Crystallogr. C* **2015**, *71*, 3–8. [[CrossRef](#)]
34. Momma, K.; Izumi, F. VESTA3 for three-dimensional visualization of crystal, volumetric and morphology data. *J. Appl. Crystallogr.* **2011**, *44*, 1272–1276. [[CrossRef](#)]
35. Koepnick, K.; Eschrig, H. Full-Potential Nonorthogonal Local-Orbital Minimum-Basis Band-Structure Scheme. *Phys. Rev. B* **1999**, *59*, 1743. [[CrossRef](#)]
36. Perdew, J.P.; Wang, Y. Accurate and Simple Analytic Representation of the Electron-Gas Correlation Energy. *Phys. Rev. B* **1992**, *45*, 13244. [[CrossRef](#)] [[PubMed](#)]
37. Blöchl, P.E.; Jepsen, O.; Andersen, O.K. Improved Tetrahedron Method for Brillouin-Zone Integrations. *Phys. Rev. B* **1994**, *49*, 16223. [[CrossRef](#)] [[PubMed](#)]
38. Takizawa, H.; Sato, T.; Endo, T.; Shimada, M. High-Pressure Synthesis and Crystal Structure of VGe<sub>2</sub> and Cr<sub>4</sub>Ge<sub>7</sub>. *J. Solid State Chem.* **1988**, *73*, 427–432. [[CrossRef](#)]
39. Rudometkina, M.V.; Seropegin, Y.D.; Schvyryaeva, E.E. Investigation of the Zr-V-Ge system alloys. *J. Less-Common Met.* **1988**, *138*, 263–269. [[CrossRef](#)]
40. Maas, J.; Bastin, G.F.; Van Loo, F.J.J.; Metselaar, R. The Texture in Diffusion-Grown Layers of Trialuminides MeAl<sub>3</sub> (Me = Ti, V, Ta, Nb, Zr, Hf) and VN<sub>3</sub>. *Z. Metallkd.* **1983**, *74*, 294–299.
41. Brukl, C.E.; Nowotny, H.; Benesovsky, F. Untersuchungen in den Dreistoffsystemen: V-Al-Si, Nb-Al-Si, Cr-Al-Si, Mo-Al-Si bzw. Cr(Mo)-Al-Si. *Monatsh. Chem.* **1961**, *92*, 967–980. [[CrossRef](#)]
42. Tanaka, K.; Nawata, K.; Inui, H.; Yamaguchi, M.; Koiwa, M. Refinement of Crystallographic Parameters in Refractory Metal Disilicides. *Mater. Res. Soc. Symp. Proc.* **2000**, *646*, N4.3.1. [[CrossRef](#)]
43. Rudometkina, M.V.; Seropegin, Y.D.; Gribanov, A.V.; Gusei, L.S. Phase equilibria in the Ti-Nb-Ge system at 1170K. *J. Less-Common Met.* **1989**, *147*, 239–247. [[CrossRef](#)]
44. Kubiak, R.; Horyn, R.; Broda, H.; Lukaszewicz, K. Refinement of the Crystal Structure of NbSi<sub>2</sub>, NbGe<sub>2</sub> and TaGe<sub>2</sub>. *Bull. Acad. Pol. Sci. (Ser. Sci. Chim.)* **1972**, *20*, 429–436.
45. Mattheiss, L.F. Calculated structural properties of CrSi<sub>2</sub>, MoSi<sub>2</sub>, and WSi<sub>2</sub>. *Phys. Rev. B Condens. Matter Mater. Phys.* **1992**, *45*, 3252–3259. [[CrossRef](#)]
46. Baykov, V.I.; Jerlerud Perez, R.; Korzhavyi, P.A.; Sundman, B.; Johansson, B. Structural stability of intermetallic phases in the Zr-Sn system. *Scr. Mater.* **2006**, *55*, 485–488. [[CrossRef](#)]
47. Kotur, B.Y. The Sc-Hf-Ge phase diagram for 1070K. *Russ. Metall. (Engl. Transl.)* **1991**, *3*, 211–214.
48. Jongste, J.F.; Loopstra, O.B.; Janssen, G.C.A.M.; Radelaar, S. Elastic constants and thermal expansion coefficient of metastable C49 TiSi<sub>2</sub>. *J. Appl. Phys.* **1993**, *73*, 2816–2820. [[CrossRef](#)]
49. Setton, M.; Van Der Spiegel, J. Structural and electrical properties of ZrSi<sub>2</sub> and Zr<sub>2</sub>CuSi<sub>4</sub> formed by rapid thermal processing. *J. Appl. Phys.* **1991**, *70*, 193–197. [[CrossRef](#)]
50. Weitzer, F.; Rogl, P.; Noel, H. The ternary system: Hafnium-silicon-uranium. *J. Alloys Compd.* **2005**, *387*, 246–250. [[CrossRef](#)]
51. Mudryk, Y.S.; Romaka, L.P.; Stadnyk, Y.V.; Bodak, O.I.; Fruchart, D. X-ray investigation of the R-Fe-Sn ternary systems (R = Y, Gd). *J. Alloys Compd.* **2004**, *383*, 162–165. [[CrossRef](#)]
52. Dasgupta, T.; Etourneau, J.; Chevalier, B.; Matar, S.F.; Umarji, A.M. Structural, thermal, and electrical properties of CrSi<sub>2</sub>. *J. Appl. Phys.* **2008**, *103*, 113516. [[CrossRef](#)]
53. Lue, C.S.; Su, T.H.; Xie, B.X.; Cheng, C. Comparative NMR study of hybridization effect and structural stability in D0<sub>22</sub>-type NbAl<sub>3</sub> and NbGa<sub>3</sub>. *Phys. Rev. B* **2006**, *74*, 094101. [[CrossRef](#)]
54. Kilduff, B.J.; Yanello, V.J.; Fredrickson, D.C. Defusing Complexity in Intermetallics: How Covalently Shared Electron Pairs Stabilize the FCC Variant Mo<sub>2</sub>Cu<sub>x</sub>Ga<sub>6-x</sub> (x ≈ 0.9). *Inorg. Chem.* **2015**, *54*, 8103–8110. [[CrossRef](#)]

